Variable atomic radii for continuum-solvent electrostatics calculation

Cite as: J. Chem. Phys. **129**, 014509 (2008); https://doi.org/10.1063/1.2949821
Submitted: 24 March 2008 . Accepted: 03 June 2008 . Published Online: 03 July 2008

Baojing Zhou, Manish Agarwal, and Chung F. Wong

Variable atomic radii for continuum-solvent electrostatics calculation

Baojing Zhou, Manish Agarwal, and Chung F. Wong[a)]
Department of Chemistry and Biochemistry and Center for Nanoscience, University of Missouri-Saint Louis, One University Boulevard, Saint Louis, Missouri 63121, USA

(Received 24 March 2008; accepted 3 June 2008; published online 3 July 2008)

We have developed a method to improve the description of solute cavity defined by the interlocking-sphere model for continuum-solvent electrostatics calculations. Many models choose atomic radii from a finite set of atom types or uses an even smaller set developed by Bondi [J. Phys. Chem. **68**, 441 (1964)]. The new model presented here allowed each atom to adapt its radius according to its chemical environment. This was achieved by first approximating the electron density of a molecule by a superposition of atom-centered spherical Gaussian functions. The parameters of the Gaussian functions were then determined by optimizing a function that minimized the difference between the properties from the model and those from *ab initio* quantum calculations. These properties included the electrostatics potential on molecular surface and the electron density within the core of each atom. The size of each atom was then determined by finding the radius at which the electron density associated with the atom fell to a prechosen value. This value was different for different chemical elements and was chosen such that the averaged radius for each chemical element in a training set of molecules matched its Bondi radius. Thus, our model utilized only a few adjustable parameters—the above density cutoff values for different chemical elements—but had the flexibility of allowing every atom to adapt its radius according to its chemical environment. This variable-radii model gave better solvation energy for 31 small neutral molecules than the Bondi radii did, especially for a quantum mechanics/Poisson–Boltzmann approach we developed earlier. The improvement was most significant for molecules with large dipole moment. Future directions for further improvement are also discussed. © *2008 American Institute of Physics*. [DOI: 10.1063/1.2949821]

I. INTRODUCTION

Significant changes can occur to the structure, property, and reactivity of a molecule when it is transferred from vacuum to aqueous solutions. Theoretical tools accounting for this phenomenon include both explicit-solvent (see, for example, Ref. 1) and implicit-solvent models (see, for example, Refs. 2 and 3). The latter approach is appealing for its lower computational costs, which is achieved by approximating the solvent by a continuum so that explicit sampling of many solvent configurations can be avoided.[3] Implicit-solvent models are therefore also often called continuum-solvent models (CSMs).[2] One popular CSM relies on solving the Poisson–Boltzmann (PB) equation,

$$\nabla \cdot [\epsilon(\mathbf{r}) \nabla \phi(\mathbf{r})] - \kappa^2(\mathbf{r}) \phi(\mathbf{r}) = \rho(\mathbf{r}), \quad (1)$$

where $\phi(\mathbf{r})$ is the electrostatic potential, $\epsilon(\mathbf{r})$ is the dielectric at $\mathbf{r}$, $\kappa(\mathbf{r})$ is the Debye–Hückel parameter, and $\rho(\mathbf{r})$ is the charge distribution of the solute. Different approaches have been developed to solve the PB equation and Ref. 2 gives an excellent review.

Solution of the PB equation [Eq. (1)] requires a definition for the dielectric boundary, which separates the solute from the solvent. This boundary needs to be suitably chosen to give reliable solvation energy. One can classify ways to define the dielectric boundary into four categories: (i) assuming the solute molecule to be spherical,[4–6] (ii) treating the molecule as an ellipsoid,[7–9] (iii) representing the molecule by a set of interlocking spheres centering on the atoms,[10–14] and (iv) using isodensity contour of the molecule obtained from quantum calculation.[15,16] The advantage of the spherical and ellipsoidal models is that Eq. (1) can be solved analytically but they usually do not yield accurate solvation energy for molecules with complex shapes. Recent applications have focused on using the latter two models.

This work devoted solely to further improving the interlocking-sphere model. In this model, one needs to choose a suitable radius for each atom. The Bondi radii are commonly used in which each chemical element is assigned the same radius. Bondi developed these radii for describing the size of chemical elements, not specifically for continuum electrostatics calculation.[17] One can develop a set of radii that is optimized for electrostatics calculation. For example, Nina *et al.* performed molecular dynamics simulation to obtain radial solvent charge distribution that provided initial estimate of atomic radii, and then adjusted them slightly to allow PB calculation to better reproduce results from explicit-solvent free energy calculation.[18] On the other hand, Stefanovich and Truong optimized their atomic radii to best fit experimental results.[19] By introducing one type of hydrogen, oxygen, fluorine, phosphorus, sulphur, and chlorine and two types of carbon and nitrogen, they obtained hydration energy for twenty neutral molecules to within about 1 kcal/mol of experiment.

a)Electronic mail: wongch@umsl.edu.

More sophisticated models further allowed the atomic radii to change according to their chemical environment. Allowing the radii to change in such a way can also compensate for the failure of the Poisson–Boltzmann model to describe nonlinear effects (see, for example, Ref. 20). Several models have been introduced to use more flexible atomic radii.[18,19,21–25] For example, Horvath *et al.* considered atomic radii as linear functions of MOPAC charges.[21] Because they used a classical continuum electrostatics model, the dielectric constant of the solute was also a parameter. Thus, the parameters of the equations for obtaining the atomic radii from the atomic partial charges depended on the choice of the dielectric constant. One can remove the dielectric constant of the solute as an adjustable parameter by treating the solute quantum mechanically. Barone *et al.*, for example, utilized such an approach, although they used a somewhat different method to describe the dependence of atomic radii on their chemical environment.[22]

In this work, we developed a new approach to deriving flexible atomic radii that fitted better with the quantum mechanics/Poisson–Boltzmann (QM/PB) model we developed earlier.[26,27] In this QM/PB model, we coupled a linear-scaling quantum mechanical code SIESTA (Ref. 28) with the Poisson–Boltzmann solver in UHBD.[29,30] In contrast to classical Poisson–Boltzmann models in which atomic partial charges lie completely inside the solute cavity, the electron density of the solute can extend beyond the cavity. Some models used suitable scaling to confine the total electron density to be within the solute cavity. (see, for example, Refs. 2, 22, and 31.) On the other hand, our model allowed the outlying charge to be outside the solute but treated it as immersing in a high dielectric medium of the water solvent rather than in a low dielectric of the solute. (The charge density within the solute cavity was still considered to reside in a low-dielectric medium of the solute, with dielectric constant equaled one.) Because of this different treatment of outlying charge, we could not simply transfer variable radii from other quantum mechanical or classical models into our model. We therefore developed a new approach to obtaining variable radii that were more consistent with our QM/PB model.

We began by representing molecular electron density by a superposition of atom-centered spherical Gaussians as this representation fitted naturally with UHBD (Refs. 29 and 30) that approximates a molecule by a collection of atomic spheres. We obtained the parameters of the Gaussians by requiring them to reproduce as well as possible the quantum mechanically calculated electrostatic potential (ESP) on molecular surface and the total electron density within the core region of each atom. Each spherical Gaussian function was then used to represent the electron density associated with the atom to which the function was centered. We then defined the radius of the atom to be the value at which the electron density represented by the spherical Gaussian function dropped to a prechosen cutoff value. For atoms in different chemical environment, the associated spherical Gaussian functions could spread out to different extent. Therefore, this Gaussian charge distribution model (Gaussian model in short) allowed the size of an atom in a molecule to adapt naturally to its chemical environment. In this work, we evaluated how well this model worked and gained insights into how it might be improved further.

II. GAUSSIAN MODEL FOR DERIVING ATOMIC RADII

We used a superposition of Gaussian functions centered on each atom to represent the molecular electron density,

$$\rho(\mathbf{r}) \approx \sum_i^N \rho_i^G(\mathbf{r}) = \sum_i^N \frac{q_i^e}{(\sqrt{2\pi}\sigma_i)^3} \exp\left\{-\frac{1}{2}\left(\frac{\mathbf{r}-\mathbf{R}_i}{\sigma_i}\right)^2\right\}, \tag{2}$$

where N was the total number of atoms and $\mathbf{R}_i$ was the position of the ith atom. The two parameters, q_i^e and σ_i, for each Gaussian function $\rho_i^G(\mathbf{r})$ gave, respectively, a sense of the electronic charge associated with an atom and the extent to which the electron density spreaded out. When σ_i approached 0, the Gaussian function $\rho_i^G(\mathbf{r})$ became the δ function and the Gaussian model reduced to the point-charge model.[32–34] The Gaussian model is more realistic than the point-charge model by mimicking the spreading out of the electron density beyond the atomic nuclei.

For the Gaussian model of Eq. (2), the ESP at a point around the molecule was given by

$$V_{\mathrm{el}}^G(\mathbf{r}) = \sum_i^N \frac{Z_i}{\mathbf{r}-\mathbf{R}_i} - \sum_i^N \frac{\rho_i^G(\mathbf{r}')}{\mathbf{r}-\mathbf{r}'}\mathrm{d}\mathbf{r}', \tag{3}$$

where Z_i was the nuclear charge of the ith atom and the integral was over all space. Following Refs. 32 and 33, we minimized the deviation of the ESP generated by the Gaussian model, $V_{\mathrm{el}}^G(\mathbf{r})$, from that produced by the QM charge density, $V_{\mathrm{el}}^Q(\mathbf{r})$, in a least-square manner by optimizing the following function:

$$R_1 = \frac{\Sigma_k[V_{\mathrm{el}}^Q(\mathbf{r}_k) - V_{\mathrm{el}}^G(\mathbf{r}_k)]^2}{\Sigma_k V_{\mathrm{el}}^Q(\mathbf{r}_k)^2}, \tag{4}$$

where $\mathbf{r}_k$ was the position vector of a point between 1.4 times and 2.0 times the van der Waals (vdW) surface of the molecule.

In addition, we introduced an additional constraint R_2 to require the total electron density within the core region of each atom to be comparable to that obtained from quantum mechanics,

$$R_2 = \sum_i^N \frac{[\int_{S_i}\rho^Q(\mathbf{r}) - \Sigma_j^N \int_{S_i}\rho_j^G(\mathbf{r})]^2}{[\int_{S_i}\rho^Q(\mathbf{r})]^2}, \tag{5}$$

where each integral was performed in a spherical volume S_i surrounding the ith atom, $\rho_j^G(\mathbf{r})$ was the Gaussian charge distribution centered on the jth atom, and $\rho^Q(\mathbf{r})$ was the electron density from *ab initio* QM calculation. We only calculated the integral within the core region of each atom because the electron density within this region was relatively spherical and constant—the valence region of an atom changed the most in forming molecules.

In ESP charge fitting, charges buried inside molecules are less well defined and can have unphysically large values.[33] Bayly *et al.* alleviated this problem by imposing

artificial constraints to keep the charges near zero.[33] Our R_2 constraint served a similar purpose, except by requiring the total electron density within the core region of each atom to be comparable to the quantum mechanical results rather than using an arbitrary constraint.

To optimize the set of parameters $\{q_i^e, \sigma_i\}$, we used the objective function R defined as

$$R = \alpha R_1 + (1-\alpha)R_2, \tag{6}$$

where α was used to control the relative weight associated with R_1 and R_2.

During the parameter optimization, we did not apply any explicit constraint on the net charge of the molecule because the net charge came up to be quite good without such a constraint (less than 10^{-4} esu for the 31 molecules studied here).

The Gaussian model allowed the molecular electron density to be partitioned into a superposition of atomic electron densities. The electron density associated with each atom were then used to determine the size of the atom in the molecule. This was achieved by choosing the radius $r_{i,G}$, at which the atomic electron density dropped to a user-chosen value, ρ_I^{iso}. In this work, ρ_I^{iso} was chosen such that the average radius $r_{I,\text{Bondi}}$ for each chemical element I (C, N, O, etc.), given by

$$\frac{1}{n}\sum_i^n r_{i,G} = r_{I,\text{Bondi}}, \tag{7}$$

where n was the total number of atoms belonging to chemical element I in a test set of molecules, matched with its corresponding Bondi radius.

III. SOLVATION ENERGY CALCULATION

We employed a classical continuum solvation model[35] (CCSM) and a quantum continuum solvation model[26,27,36,37] (QCSM) that we developed earlier to compute the solvation free energy of 31 small neutral molecules shown in Table I. In both the CCSM and the QCSM, the ESP $\phi(\mathbf{r})$ generated by the charge distribution of the solute molecule was calculated by solving the PB equation [Eq. (1)],[38,39] with the finite difference method.[40] The reaction field $\phi_{\text{RF}}(\mathbf{r})$ was obtained by

$$\phi_{\text{RF}}(\mathbf{r}) = \phi_{\text{solvent}}(\mathbf{r}) - \phi_{\text{vac}}(\mathbf{r}), \tag{8}$$

where $\phi_{\text{solvent}}(\mathbf{r})$ and $\phi_{\text{vac}}(\mathbf{r})$ were the electrostatic potential obtained by solving the PB equation in solvent and in vacuum, respectively. The dielectric boundary between the solute and the water solvent was defined by using the vdW surface. The solvation free energy G_{sol} included the electrostatic G_{el} and the nonpolar contributions G_{np},[35,36]

$$G_{\text{sol}} = G_{\text{el}} + G_{\text{np}}. \tag{9}$$

G_{np} was evaluated as a surface area dependent term,[35]

$$G_{\text{np}} = \sigma A, \tag{10}$$

where A was the solvent accessible surface (SAS) area[41] and σ was a surface tension coefficient set to 0.006 kcal/mol Å^{-2} in this work.

The CCSM differed from the QCSM mainly in the treatment of the solute molecule. In the CCSM, the solute was represented by point charges located at atomic centers.[35] The electrostatic energy G_{el} was computed via[35]

$$G_{\text{el}} = \frac{1}{2}\sum_i q_i \phi_{\text{RF},i}, \tag{11}$$

where q_i and $\phi_{\text{RF},i}$ were the point charge and the reaction field at the ith atom, respectively.

On the other hand, the QCSM provided a more rigorous description of the solute, for which the QM charge density was directly used.[26,36,37] One widely used *ab initio* QM method to calculate the electron density is the Kohn–Sham density functional theory (KS-DFT),[42,43] in which one solves the following KS equation (in hartree atomic units):

$$\left(-\tfrac{1}{2}\nabla^2 + v_{\text{eff}}^{\text{KS}}[\rho](\mathbf{r}) + \phi_{\text{RF}}(\mathbf{r})\right)\psi_i(\mathbf{r}) = \epsilon_i \psi_i(\mathbf{r}). \tag{12}$$

Here, ϵ_i is the eigenvalue of the ith orbital, $\psi_i(\mathbf{r})$, and the KS effective potential $v_{\text{eff}}^{\text{KS}}[\rho](\mathbf{r})$ contains the Hartree, the exchange-correlation (XC), and the ion-electron potentials,

$$\begin{aligned} v_{\text{eff}}^{\text{KS}}[\rho](\mathbf{r}) &= \frac{\delta E_H[\rho]}{\delta\rho(\mathbf{r})} + \frac{\delta E_{\text{xc}}[\rho]}{\delta\rho(\mathbf{r})} + v_{\text{ne}}(\mathbf{r}) \\ &= v_H[\rho](\mathbf{r}) + v_{\text{xc}}[\rho](\mathbf{r}) + v_{\text{ne}}(\mathbf{r}). \end{aligned} \tag{13}$$

The electron density is generated via

$$\rho(\mathbf{r}) = \sum_i f_i |\psi_i(\mathbf{r})|^2, \tag{14}$$

where f_i is the occupation number of $\psi_i(\mathbf{r})$. Since Eqs. (1), (8), and (12) are coupled, we solved them iteratively until self-consistency was reached.[26,27] In the QCSM, the electrostatic energy G_{el} was given by

$$G_{\text{el}} = G_{\text{RF}} + G_{\text{wfd}}, \tag{15}$$

where G_{RF} was the electrostatic interaction energy between the solute and the reaction field,

$$G_{\text{RF}} = \frac{1}{2}\int \rho(\mathbf{r})\phi_{\text{RF}}(\mathbf{r})d\mathbf{r} + \tfrac{1}{2}\sum_i Z_i \phi_{\text{RF}}(\mathbf{r}), \tag{16}$$

and G_{wfd} was the energy associated with the distortion of the wave function in transferring the solute from vacuum to solution,[36]

$$G_{\text{wfd}} = \langle \Psi^s | H^0 | \Psi^s \rangle - \langle \Psi^g | H^0 | \Psi^g \rangle. \tag{17}$$

Here Ψ^g was the gas-phase solute wave function, Ψ^s was the solvated solute wave function, and H^0 was the gas-phase Hamiltonian.

IV. CALCULATIONAL DETAIL

The geometry of the 31 small neutral molecules (see Table I) in the gas phase were optimized by all-electron KS-DFT calculations with GAUSSIAN03,[44] using the 6-31G(d) basis set. We also used the Becke3LYP functional[45–48] for the electron XC. Then, the QM charge density and the corresponding ESP were generated on fine grids of 6–8 points/bohr using the "*cubgen*" utility of GAUSSIAN03 in order to determine the parameters of the Gaussian model. We

TABLE I. Experimental and calculated hydration free energies for 31 small neutral molecules (in kcal/mol). The number under each molecule's name was the gas-phase dipole moment (in debye).

Molecule	Model	G_{RF}	G_{wfd}	G_{np}	G_{sol}	Exptl.	Molecule	Model	G_{RF}	G_{wfd}	G_{np}	G_{sol}	Exptl.
Methane	C/B	−0.34		0.86	0.52	1.93	acetonitrile	C/B	−7.34		1.09	−6.25	−3.90
	C/G	−0.36		0.85	0.49			C/G	−7.59		1.08	−6.51	
0.00	Q/B	−0.75	−0.03	0.86	0.08		3.75	Q/B	−9.32	2.24	1.09	−5.98	
	Q/G	−0.98	−0.02	0.85	−0.15			Q/G	−10.18	2.43	1.08	−6.67	
butane	C/B	−0.24		1.54	1.30	2.15	acetic acid	C/B	−10.27		1.19	−9.08	−6.70
	C/G	−0.17		1.61	1.44			C/G	−10.41		1.19	−9.22	
0.01	Q/B	−1.55	0.08	1.54	0.08		4.12	Q/B	−11.49	2.55	1.19	−7.75	
	Q/G	−0.87	0.10	1.61	0.84			Q/G	−11.86	2.62	1.19	−8.05	
i-butane	C/B	−0.44		1.48	1.04	2.30	propionic acid	C/B	−9.96		1.38	−8.59	−6.47
	C/G	−0.31		1.56	1.25			C/G	−10.00		1.39	−8.60	
0.06	Q/B	−1.64	0.11	1.48	−0.06		4.24	Q/B	−11.90	2.50	1.38	−8.03	
	Q/G	−1.10	0.08	1.56	0.55			Q/G	−12.07	2.53	1.39	−8.14	
n-butylamine	C/B	−5.48		1.66	−3.82	−4.29	benzene	C/B	−3.03		1.41	−1.61	−0.90
	C/G	−5.07		1.66	−3.41			C/G	−3.06		1.40	−1.66	
1.44	Q/B	−5.73	0.71	1.66	−3.35		0.01	Q/B	−2.46	0.28	1.41	−0.77	
	Q/G	−5.40	0.68	1.66	−3.06			Q/G	−2.82	0.32	1.40	−1.10	
methylamine	C/B	−5.41		1.02	−4.39	−4.50	toluene	C/B	−2.52		1.57	−0.94	0.90
	C/G	−5.81		1.03	−4.77			C/G	−2.54		1.59	−0.95	
1.57	Q/B	−4.86	0.69	1.02	−3.14		0.32	Q/B	−3.20	0.39	1.57	−1.24	
	Q/G	−5.44	0.76	1.03	−3.64			Q/G	−3.64	0.44	1.59	−1.61	
ethanol	C/B	−5.39		1.20	−4.19	−5.01	4-cresol	C/B	−6.91		1.65	−5.27	−6.13
	C/G	−4.84		1.26	−3.58			C/G	−7.07		1.69	−5.38	
1.61	Q/B	−5.65	0.74	1.20	−3.70		1.27	Q/B	−6.81	1.01	1.65	−4.16	
	Q/G	−5.25	0.74	1.26	−3.26			Q/G	−7.44	1.10	1.69	−4.65	
methyl ethyl	C/B	−3.56		1.57	−1.99	−1.49	phenol	C/B	−6.90		1.45	−5.45	−6.60
sulfide	C/G	−3.56		1.60	−1.96			C/G	−7.01		1.46	−5.54	
1.71	Q/B	−4.16	0.51	1.57	−2.08		1.31	Q/B	−6.71	1.02	1.45	−4.23	
	Q/G	−4.13	0.51	1.60	−2.02			Q/G	−7.10	1.07	1.46	−4.57	
methanethiol	C/B	−3.45		1.12	−2.32	−1.24	aniline	C/B	−7.55		1.46	−6.09	−5.49
	C/G	−3.43		1.13	−2.31			C/G	−8.59		1.49	−7.10	
1.75	Q/B	−3.24	0.36	1.12	−1.75		2.06	Q/B	−7.67	1.32	1.46	−4.90	
	Q/G	−3.26	0.36	1.13	−1.76			Q/G	−9.99	1.73	1.49	−6.77	
methanol	C/B	−5.43		0.98	−4.46	−5.11	3-methyl-	C/B	−6.87		1.89	−4.98	−5.91
	C/G	−5.53		0.98	−4.54		indole	C/G	−7.29		1.87	−5.42	
1.78	Q/B	−4.94	0.71	0.98	−3.25		2.11	Q/B	−7.99	1.50	1.89	−4.60	
	Q/G	−5.02	0.72	0.98	−3.32			Q/G	−9.40	1.75	1.87	−5.77	
ethanethiol	C/B	−3.25		1.28	−1.97	−1.30	pyridine	C/B	−5.14		1.37	−3.77	−4.70
	C/G	−2.68		1.35	−1.33			C/G	−5.19		1.35	−3.83	
1.85	Q/B	−4.00	0.42	1.28	−2.31		2.13	Q/B	−6.21	1.16	1.37	−3.69	
	Q/G	−3.36	0.35	1.35	−1.67			Q/G	−6.67	1.24	1.35	−4.07	
NH_3	C/B	−7.19		0.80	−6.39	−4.29	9-methyl-	C/B	−15.66		1.91	−13.76	−13.6
	C/G	−7.74		0.74	−7.00		adenine	C/G	−15.81		1.88	−13.93	
1.94	Q/B	−5.82	0.82	0.80	−4.20		2.49	Q/B	−17.66	2.96	1.91	−12.79	
	Q/G	−6.84	0.94	0.74	−5.16			Q/G	−18.66	3.10	1.88	−13.68	
H_2O	C/B	−7.76		0.74	−7.02	−6.30	4-methyl-	C/B	−9.59		1.49	−8.10	−10.25
	C/G	−7.76		0.74	−7.02		imidazole	C/G	−9.99		1.48	−8.51	
2.10	Q/B	−6.32	0.87	0.74	−4.71		3.29	Q/B	−12.14	2.88	1.49	−7.78	
	Q/G	−6.30	0.85	0.74	−4.72			Q/G	−13.43	3.12	1.48	−8.82	
n-propyl-	C/B	−13.47		1.82	−11.65	−10.91	1-methyl-	C/B	−13.75		1.67	−12.09	−14.0
guanidine	C/G	−14.61		1.76	−12.85		uracil	C/G	−14.30		1.63	−12.67	
2.52	Q/B	−14.52	2.83	1.82	−9.87		4.48	Q/B	−17.54	3.57	1.67	−12.30	
	Q/G	−17.05	3.31	1.76	−11.98			Q/G	−18.98	3.79	1.63	−13.56	
acetone	C/B	−5.22		1.36	−3.86	−3.90	l-methyl-	C/B	−16.51		1.71	−14.80	−18.40
	C/G	−5.32		1.34	−3.98		cytosine	C/G	−17.62		1.69	−15.92	
2.73	Q/B	−6.90	1.35	1.36	−4.19		5.67	Q/B	−21.35	5.41	1.71	−14.23	
	Q/G	−7.39	1.43	1.34	−4.63			Q/G	−23.86	5.93	1.69	−16.23	
acetamide	C/B	−10.27		1.24	−9.03	−9.71	9-methyl-	C/B	−21.66		1.97	−19.69	−22.4
	C/G	−11.04		1.20	−9.84		guanine	C/G	−22.60		1.98	−20.62	
3.57	Q/B	−12.39	2.59	1.24	−8.56		6.65	Q/B	−27.67	6.47	1.97	−19.24	

TABLE I. (*Continued.*)

Molecule	Model	G_{RF}	G_{wfd}	G_{np}	G_{sol}	Exptl.	Molecule	Model	G_{RF}	G_{wfd}	G_{np}	G_{sol}	Exptl.
	Q/G	−14.46	2.95	1.20	−10.32			Q/G	−30.04	6.98	1.98	−21.08	
propionamide	C/B	−10.02		1.42	−8.61	−9.41	RMS	C/B		1.46			
	C/G	−10.67		1.40	−9.27		error	C/G		1.40			
3.64	Q/B	−12.24	2.51	1.42	−8.31			Q/B		1.71			
	Q/G	−13.72	2.75	1.40	−9.57			Q/G		1.38			

used the simplex method[49] to minimize R in Eq. (6) with respect to the parameter set $\{q_i^e, \sigma_i\}$. The atomic point charges derived from the Merz–Kollman scheme[32] and half the Bondi radii[17] were used as initial guesses for $\{q_i^e\}$ and $\{\sigma_i\}$, respectively. Then, the resulting Gaussian models for all the 31 small neutral molecules were used to determine the cutoff density ρ^{iso} for each chemical element so that Eq. (7) was satisfied.

The PB equation was solved by using the University of Houston Brownian dynamics[29,30] (UHBD) program. We used the vdW surface to define the dielectric boundary between the solute and the water solvent. To determine the vdW surface, we either used the Bondi radii, or the more flexible atomic radii from our Gaussian model. The dielectric $\epsilon(\mathbf{r})$ was set to 1 for gas-phase calculations. In solution, the dielectric was set to 1 inside the vdW surface and 78 for the water solvent. The focusing method was used to solve the PB equation in which we first used a coarse grid with a spacing of 0.5 Å followed by a fine grid with a grid spacing of 0.25 Å. The SAS,[41] which was constructed by rolling a probe sphere with a radius of 1.4 Å on the vdW surface, was used to evaluate the nonpolar contribution to the solvation energy according to Eq. (10).

We used both the CCSM (Ref. 35) and the QCSM (Refs. 26, 36, and 37) to compute solvation free energy for comparison. In the CCSM, we used the Merz-Kollman point charges[32] but increased them by 16% in order to mimic polarization effect by the solvent, as done previously by Honig and co-workers.[35] In the QCSM, we solved the coupled KS and PB equations self-consistently with a modified SIESTA code.[27,28] In the KS-DFT calculations, we used the Becke3LYP density functional[45–48] and the nonlocal pseudopotential of Troullier and Martins.[50] The default double-ζ plus single polarization basis set in SIESTA was used and the grid cutoff was set to 100 Rydberg.

V. RESULTS AND DISCUSSIONS

A. Atomic radii from the Gaussian model

We first determined the values of the two model parameters, S_i and α in Eqs. (5) and (6), which gave good fit between the Gaussian model and results from QM calculations. For this, S_i was expressed as the percent vdW volume of the ith atom calculated by using the Bondi radius of the atom. By calculating R as a function of α and S_i for methanol and benzene, we found that S_i=40% and α=0.6 gave good agreement between our Gaussian model and the QM results. Then, by fixing S_i and α to these values, we optimized q_i and σ_i to minimize R for the 31 neutral molecules listed in Table I. To facilitate analysis, we divided the 31 molecules into three groups: acyclic compounds (molecules 1–19), carbocyclic compounds (molecules 20–24), and heterocyclic compounds (molecules 25–31). Within each group, the molecules were ordered with increasing dipole moment (see Table I).

We compared the relative root mean square (RRMS) error of the ESP (measured by $\sqrt{R_1}$) from our Gaussian model and from the Merz–Kollman point-charge model[32] in Fig. 1(a). For the acyclic compounds with small dipole moments (molecules 1–19), the ESPs produced by our Gaussian model and the Merz–Kollman point-charge model exhibited large deviations from those generated by QM charge density.

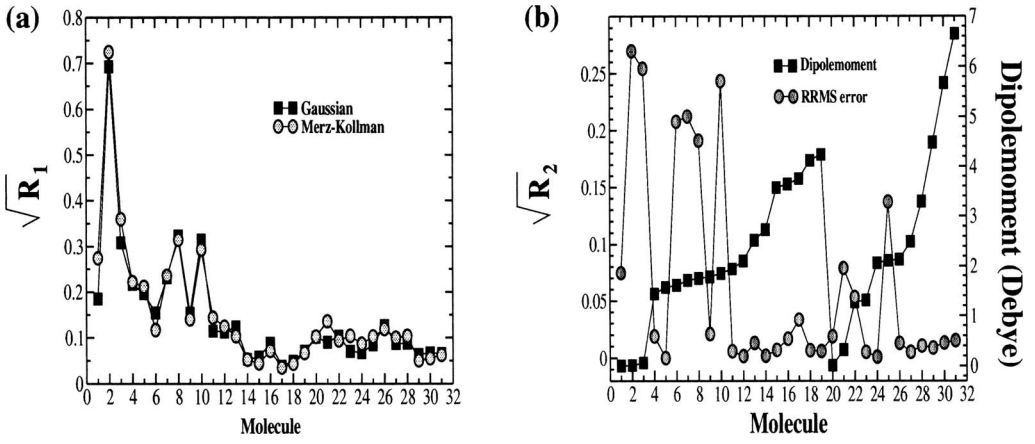

FIG. 1. (a) RRMS error of the electrostatic potential [$\sqrt{R_1}$ of Eq. (4)] for the Gaussian model (solid square) and Merz–Kollman model (opaque circle) for 31 neutral molecules. (b) RRMS error for the total number of electrons in atomic core [$\sqrt{R_2}$ of Eq. (5)] (opaque circle). Solid squares were the calculated dipole moments of the molecules. The molecules are arranged in the order shown in Table I.

TABLE II. Bondi radii r_{Bondi}, the density cutoffs ρ^{iso} for determining atomic radii, and the standard deviations (s.d.) from the means, which were the Bondi radii in our model.

	C	H	O	N	S
r_{Bondi} (Å)	1.70	1.20	1.52	1.55	1.80
ρ^{iso} (a.u.)	0.0057	0.0013	0.0028	0.0059	0.0253
s.d. (a.u.)	0.061	0.21	0.028	0.025	0.0053

The largest error ($\sqrt{R_1} \approx 0.7$) came from the nonpolar molecule butane. With increasing dipole moment, the error in the ESP for the acyclic compounds decreased except for the sulphur-containing compounds methyl ethyl sulfide, methanethiol, and ethanethiol. For carbocyclic compounds (molecules 20–24), the ESP obtained from QM charge density was much better reproduced. The third group, heterocyclic compounds having the largest dipole moments [2–7 debye, see Fig. 1(b)] among the molecules studied (molecules 25–31), reproduced the ESP obtained from the QM charge density very well by both models, with $\sqrt{R_1}$ less than 0.15. Overall, our Gaussian model reproduced the ESP to the same quality as the Merz–Kollman point-charge model did.

The RRMS errors for the total number of electrons in the atomic core (measured by $\sqrt{R_2}$ from the Gaussian model are illustrated in Fig. 1(b). The largest error ($\sqrt{R_1} \approx 0.28$) was found again for the nonpolar butane. The RRMS errors were also large ($\sqrt{R_2} \geqslant 0.05$) for 7 acyclic compounds, 2 carbocyclic compounds, and 1 heterocyclic compound. As mentioned before, R_2 was mainly used to prevent unphysically large charge for buried atoms. We did not expect superior match between the Gaussian model and quantum mechanical results as the single-spherical-Gaussian representation was still relatively crude in describing atomic electron density in molecule. This contraint model was just a bit more appealing than using arbitrary constraints such as artificially requiring atomic charges to be near zero.

We derived the atomic radii from the Gaussian model using the scheme described in Sec. II. Table II presents the Bondi radii and the density cutoff value ρ^{iso} that was found to reproduce them in an averaged sense for the 31 molecules studied here. For all the five chemical elements, C, H, O, N, and S, the cutoff values were larger than the 0.001 a.u. previously used in determining molecular cavity from isodensity contour.[15,16] The discrepancy is not surprising as the two models are rather different. In our Gaussian model, we approximated the molecular electron density by a superposition of spherical Gaussians centering on atoms, and then used the "radius" at which the electron density dropped to the chosen cutoff value to define the radius of each atom. (The cutoff density could be different for different chemical elements.) The atomic radii obtained were then used to construct the van der Waals surface for defining the dielectric boundary in Poisson–Boltzmann calculation. On the other hand, the other model utilized isoelectron density obtained from QM calculation of a molecule to define molecular cavity. A fixed value of the isoelectron density was used for every point on the surface independent of which chemical element the point was closest to.[15,16]

Because the chemical environment could be different for different atoms, atoms belonging to the same chemical element could have different radii in the same molecule in our Gaussian model. Table II shows the standard deviation of the radius for each of the five chemical elements obtained from the 31 molecules studied here. Hydrogen demonstrated the largest fluctuation among these chemical elements.

B. Solvation energy calculation

Having developed a more flexible way of determining the atomic radii, we then examined whether their use could improve the calculation of hydration energy. The results for 31 neutral molecules are shown in Table I for four models: C/B, C/G, Q/B, and Q/G. Here, C and Q represent the CCSM and the QCSM, respectively, and B and G refer to using Bondi radii and atomic radii from our Gaussian model, respectively. The gas-phase dipole moments of these molecules obtained from the KS-DFT calculations using the Becke3LYP functional and the 6-31G(d) basis set are also shown.

Table I shows that using our variable radii in both the CCSM and the QCSM calculations led to more negative (i.e., favorable) electrostatics energy G_{el} [see Eq. (9)] for most molecules, especially those with large dipole moments μ. In the CCSM, the largest change in G_{el} was about -1.0 kcal/mol and was found in *n*-propyl-guanidine, aniline, 1-methyl-cytosine, and 9-methyl-guanine. In the QCSM, G_{el} contained two terms: G_{RF} and G_{wfd}. The largest change in G_{RF} was about -2.5 kcal/mol and was again observed for the above four molecules. The wave function distortion energy was also larger when G_{el} became more negative, although the change was comparatively small (the maximum was about 0.5 kcal/mol found in 1-methyl-cytosine). The nonpolar energy G_{np} [Eq. (10)] was much less affected by the choice of atomic radii. Overall, our variable radii produced better hydration free energy than the Bondi radii did, and the improvement was more significant for the QCSM than the CCSM. The root mean square (RMS) error was reduced by $\sim$0.3 kcal/mole for the former and by $\sim$0.1 kcal/mole for the latter (the RMS errors for the four models are shown at the bottom of Table I). The correlation coefficients between calculated and experimental results for the four models were 0.97.

In both the CCSM and the QCSM, the reaction field $\phi_{\text{RF}}(\mathbf{r})$ was quite sensitive to the shape and size of the molecular cavity. However, there were subtle differences between the two models. In the CCSM, the point charges always laid inside the solute cavity. On the other hand, the QCSM always produced a small amount of solute charge density outside the cavity because the QM charge density could extend over all space in our model. The charge density was treated differently depending on whether it was inside or outside the cavity. If outside, it was considered to be in a region of high dielectric of the water solvent; if inside, it was considered to be in a region of low dielectric of the solute. Because of this treatment, the calculated results could be more sensitive to the choice of atomic radii and our calcula-

TABLE III. Average atomic radii (r_{ave}) of H atoms that were bounded to O (H^a), N (H^b), and other atoms (H^c) and the standard deviations (s.d.) from the mean, which was the Bondi radius.

	H^a	H^b	H^c
r_{ave} (Å)	1.20	1.14	1.21
s.d. (a.u.)	0.0082	0.21	0.22

tions showed that the variable-radii model improved calculated solvation energy more significantly for the QCSM.

The largest difference between the cavity defined by our variable atomic radii and that defined by the Bondi radii mainly arised from the hydrogens, as indicated by its much larger deviation in Table II. To gain further insight, we divided the hydrogens into three groups according to the type of element they were bounded to: oxygen, nitrogen, or others. The average radii r_{ave}, and their standard deviations are compared in Table III. The averaged radius of hydrogens bonded to chemical elements with lower electronegativity, such as carbon and sulphur, was slightly larger than the Bondi radius. In contrast, hydrogens bonded to the more electronegative nitrogens shrinked significantly by ~0.06 Å. However, this correlation between electronegativity and atomic radius ended when we examined hydrogens connected to the electronegative oxygens (we only considered hydroxyl oxygen at this time)—their average radii were comparable to the Bondi radius.

Empirical force fields usually have different radii for hydroxyl hydrogens and hydrogens attached to less electronegative atoms. For example, in the AMBER force field, the hydroxyl hydrogen adopted a smaller radius, 1.0 Å, than hydrogens bonded to carbon, 1.38 Å.[51] Tawa *et al.* also used more than one hydrogen types in their PB approach that combined with semi-empirical molecular orbital theory,[52] Hartree–Fock theory, or *ab initio* DFT.[53] On the other hand, the radii of hydroxyl hydrogens in our Gaussian model had similar values to those attached to carbons. This might be because our single-Gaussian model with a single density cutoff might not be flexible enough to describe the size variation for each chemical element. A close inspection of the data in Table I disclosed that the solvation energy of the five alcohols was systematically underestimated by the Q/G model. This observation motivated us to try a smaller atomic radius for the hydroxyl hydrogens. We found that a smaller radius of 1.08 Å reproduced the experimental solvation energy of water well. This corresponded to a cutoff density ρ^{iso} of 0.003 a.u. If we repeated the solvation energy calculations using this new cutoff density for hydroxyl hydrogens, we found that the results were improved for both the C/G and the Q/G models. In the following, we refer these two models as C/G/H* and Q/G/H* to distinguish them from the previous C/G and Q/G models. As seen from Table IV, the experimental solvation energy was much better reproduced for the alcohols by the C/G/H* model (the result for water worsened a bit because the cutoff was optimized for the Q/G/H* model). On the other hand, the solvation energy for water and all the alcohols in this study was improved by the Q/G/H* model. The RMS errors were only 0.89 and 0.71 kcal/mol for the C/G/H* and the Q/G/H* models, respectively.

Note that we had not applied the above treatment to hydroxyl hydrogens in carboxylate groups because the calculated solvation energy was already too negative for both the C/G and the Q/G models. Reducing the size of these hydroxyl hydrogens would most likely worsen the results further. This analysis showed that our model using one single Gaussian and one single density cutoff was not flexible enough to describe the size variation of hydrogens attaching to different types of heavier elements adequately. For further improvement, one might use a sum of Gaussians to represent the density of each atom-in-the-molecule but this will increase the number of parameters to be optimized in Eq. (6). A cheaper alternative might be to use different cutoff radii for hydrogens attaching to different types of heavy atoms. Before such refinement is made, the Q/G/H* model is preferred over the Q/G model.

To gain further insights into which groups of compounds might benefit more from the refined model, we divided the 31 compounds into three subsets based on the magnitude of their dipole moments, μ. Molecules with $\mu < 1.0$ debye were in subset 1, those with $1.0 \leqslant \mu < 3.0$ debye were in subset 2, and the remaining molecules with $\mu \geqslant 3.0$ debye were in subset 3. The number of molecules in subsets 1, 2, and 3 were 5, 17, and 9, respectively. We reevaluated the RMS error in the hydration energy for these three subsets of molecules separately and the results are shown in Table V. For molecules in subset 1, the variable-radii model reduced the RMS error by approximately 0.04 kcal/mol when the the CCSM was used. A better improvement of 0.13 kcal/mol was obtained for the QCSM. The RMS errors for molecules in subset 2 for the six calculational models were smaller than those in subsets 1 and 3. The C/G model increased the RMS error by 0.26 kcal/mol relative to the C/B model. Using the C/G/H* model reduced the RMS error from the C/G model

TABLE IV. Hydration free energies of water and alcohols (in kcal/mol) from classical and quantum PB calculations using a refined density cutoff of 0.003 a.u. for the hydroxyl hydrogens.

Molecule	Model	G_{RF}	G_{wfd}	G_{np}	G_{sol}	Exptl.	Molecule	Model	G_{RF}	G_{wfd}	G_{np}	G_{sol}	Exptl.
methanol	C/G/H*	−6.08		0.98	−5.10	−5.11	phenol	C/G/H*	−7.78		1.44	−6.33	−6.60
	Q/G/H*	−6.09	0.91	0.98	−4.20			Q/G/H*	−8.55	1.39	1.44	−5.72	
H_2O	C/G/H*	−8.76		0.70	−8.06	−6.30	ethanol	C/G/H*	−5.40		1.25	−4.15	−5.01
	Q/G/H*	−8.23	1.13	0.70	−6.40			Q/G/H*	−6.32	0.92	1.25	−4.14	
4-cresol	C/G/H*	−7.83		1.68	−6.15	−6.13	RMS	C/G/H*		0.89			
	Q/G/H*	−8.79	1.38	1.68	−5.72		error	Q/G/H*		0.71			

TABLE V. RMS error (in kcal/mol) of the hydration energy of the molecules in Table I divided into three subsets according to the magnitude of their dipole moments μ (in Debye).

	C/B	C/G	C/G/H*	Q/B	Q/G	Q/G/H*
Set 1 ($\mu<1.0$)	1.28	1.24	1.24	1.89	1.76	1.76
Set 2 ($1.0\leqslant\mu<3.0$)	0.87	1.13	1.11	1.25	1.15	0.76
Set 3 ($\mu\geqslant3.0$)	2.24	1.88	1.88	2.28	1.54	1.54
Total	1.46	1.40	1.40	1.71	1.38	1.22

by only 0.02 kcal/mol. On the other hand, the improvement by using the variable-radii model was more significant for the QCSM. The reduction of RMS error was ~0.1 and ~0.5 kcal/mol for the Q/G and Q/G/H* models, respectively. The variable-radii model gave the largest improvement for subset 3, which included molecules with the highest dipole moment in this study. The reduction of RMS error was ~0.36 kcal/mol for the CCSM and ~0.64 kcal/mol for the QCSM. Finally, among all the models studied here, the Q/G/H* model produced the best results with a total RMS error of 1.22 kcal/mol.

VI. CONCLUSIONS

We have developed a new method for deriving atomic radii that are more flexible for continuum electrostatics calculation. The method was based on representing molecular electron density by a superposition of spherical Gaussians centering on the atoms. The parameters of the Gaussians were optimized to reproduce the quantum mechanical electrostatic potential on molecular surface and the core electron density of each atom. After determining the parameters of the Gaussian functions, the radius of each atom in the molecule was determined by the radius at which the electron density dropped to a suitable cutoff. This cutoff was simply chosen such that the averaged radii for each chemical element in a training set of molecules matched the corresponding Bondi radius. This variable-radii model also allowed nonlinear effects to be described more readily in continuum-solvent models. In testing this model on calculating the hydration energy of thirty one neutral molecules, we found better results for both the classical Poisson–Boltzmann model and the quantum mechanics/Poisson–Boltzmann model we developed earlier, although the improvement was more significant for the latter quantum model in which electron charge was allowed to extend beyond the solute into the higher dielectric solvent. Furthermore, the model improved the results for polar molecules more than less polar ones.

Our study also revealed limitations that can be further improved in the future. We found that the solvation energy of water and alcohols were systematically underestimated by the quantum mechanics/Poisson–Boltzmann model using our variable atomic radii. Reducing the atomic radii by ~0.1 Å for hydroxyl hydrogens significantly improved the solvation energy for these compounds. The failure of our current model to adequately describe the size of hydroxyl hydrogens might stem from the relatively simple one-Gaussian representation of the atomic electron density. Including more Gaussians might improve the results but with increased expenses to obtain the parameters and coefficients of the Gaussians. A cheaper alternative might be to use more than one density cutoff for hydrogens depending on what types of heavy atoms they are bonded to. Furthermore, in this work, we simply estimated the cutoff electron densities for different chemical elements by finding values that made the averaged atomic radii of a training set of molecules comparable to the Bondi radii. Choosing cutoff electron densities that best reproduce the hydration energy of a training set of molecules should further improve the model.

ACKNOWLEDGMENTS

This research was supported by the U.S. National Institutes of Health, a Research Award from the University of Missouri-Saint Louis, and a Research Board Award from the University of Missouri System.

[1] C. L. Brooks III, M. Karplus, and B. M. Pettitt, in *Advances in Chemical Physics*, edited by I. Prigogine and S. A. Rice (Wiley, New York, 1988), Vol. LXXI.
[2] J. Tomasi, B. Mennucci, and R. Cammi, Chem. Rev. (Washington, D.C.) **105**, 2999 (2005).
[3] C. J. Cramer and D. G. Truhlar, Chem. Rev. (Washington, D.C.) **99**, 2161 (1999).
[4] L. Onsager, J. Am. Chem. Soc. **58**, 1486 (1936).
[5] M. Born, Z. Phys. **1**, 45 (1920).
[6] J. G. Kirkwood, J. Chem. Phys. **2**, 351 (1934).
[7] F. H. Westheimer and J. G. Kirkwood, J. Chem. Phys. **6**, 513 (1938).
[8] S. W. Harrison, H.-J. Nolte, and D. L. Beveridge, J. Phys. Chem. **80**, 2580 (1976).
[9] J.-L. Rivail and B. Terryn, J. Chem. Phys. **79**, 1 (1982).
[10] M.-J. Huron and P. Claverie, J. Phys. Chem. **76**, 2123 (1972); **78**, 1853 (1974).
[11] B. Lee and F. M. Richards, J. Mol. Biol. **55**, 379 (1971).
[12] B. Honig, K. Sharp, and A. Yang, J. Phys. Chem. **97**, 1101 (1993).
[13] J. L. Chen, L. Noodleman, D. A. Case, and D. Bashford, J. Phys. Chem. **98**, 11059 (1994).
[14] X. Song and D. Chandler, J. Chem. Phys. **108**, 2594 (1998).
[15] J. B. Foresman, T. A. Keith, K. B. Wiberg, J. Snoonian, and M. J. Frisch, J. Phys. Chem. **100**, 16098 (1996).
[16] C. G. Zhan and D. M. Chipman, J. Chem. Phys. **109**, 10543 (1998).
[17] A. Bondi, J. Phys. Chem. **68**, 441 (1964).
[18] M. Nina, D. Beglov, and B. Roux, J. Phys. Chem. B **101**, 5239 (1997).
[19] E. V. Stefanovich and T. N. Truong, Chem. Phys. Lett. **244**, 65 (1995).
[20] S. W. Rick and B. J. Berne, J. Am. Chem. Soc. **116**, 3949 (1994).
[21] D. Horvath, D. Van Belle, G. Lippens, and S. J. Wodak, J. Chem. Phys. **104**, 6679 (1996).
[22] V. Barone, M. Cossi, and J. Tomasi, J. Chem. Phys. **107**, 3210 (1997).
[23] B. Marten, K. Kim, C. Cortis, R. Friesner, R. B. Murphy, M. N. Ringnalda, D. Sitkoof, and B. Honig, J. Phys. Chem. **100**, 11775 (1996).
[24] J. S. Bader, C. M. Cortis, and B. J. Berne, J. Chem. Phys. **106**, 2372 (1997).
[25] M. A. Aguilar and F. J. Olivares del Valle, Chem. Phys. **129**, 439 (1989).
[26] M. Wang and C. F. Wong, J. Phys. Chem. A **110**, 4873 (2006).
[27] M. Wang, C. F. Wong, J. Liu, and P. Zhang, Chem. Phys. Lett. **442**, 464 (2007).
[28] J. M. Soler, E. Artacho, J. D. Gale, A. García, J. Junquera, P. Ordejón, and D. Sánchez-Portal, J. Phys.: Condens. Matter **14**, 2745 (2002).
[29] M. E. Davis, J. D. Madura, B. A. Luty, and J. A. McCammon, Comput. Phys. Commun. **62**, 187 (1991).
[30] J. D. Madura, J. M. Briggs, R. C. Wade *et al.*, Comput. Phys. Commun. **91**, 57 (1995).
[31] B. Mennucci and J. Tomasi, J. Chem. Phys. **106**, 5151 (1997).
[32] B. H. Besler, K. M. Merz, and P. A. Kollman, J. Comput. Chem. **11**, 431 (1990).
[33] C. I. Bayly, P. Cieplak, W. D. Cornell, and P. A. Kollman, J. Phys. Chem. **97**, 10269 (1993).
[34] C. M. Breneman and K. B. Wiberg, J. Comput. Chem. **11**, 361 (1990).
[35] D. Sitkoff, K. A. Sharp, and B. Honig, J. Phys. Chem. **98**, 1978 (1994).

[36] D. J. Tannor, B. Marten, R. Murphy, R. A. Friesner, D. Sitkoff, A. Nicholls, M. Ringnalda, W. A. Goddard III, and B. Honig, J. Am. Chem. Soc. **116**, 11875 (1994).
[37] V. Gogonea and K. M. Merz, J. Phys. Chem. A **103**, 5171 (1999).
[38] K. A. Sharp and B. Honig, J. Phys. Chem. **94**, 7684 (1990).
[39] M. E. Davis and J. A. McCammon, Chem. Rev. (Washington, D.C.) **90**, 509 (1990).
[40] B. A. Luty, M. E. Davis, and J. A. McCammon, J. Comput. Chem. **13**, 1114 (1992).
[41] F. A. Richards, Annu. Rev. Biophys. Bioeng. **6**, 151 (1977).
[42] R. G. Parr and W. Yang, *Density-Functional Theory of Atoms and Molecules* (Clarendon, New York, 1989); R. M. Dreizler and E. K. U. Gross, *Density Functional Theory: An Approach to the Quantum Many-Body Problem* (Springer-Verlag, Berlin, 1990).
[43] W. Kohn and L. J. Sham, Phys. Rev. **140**, A1133 (1965).
[44] M. J. Frisch, G. W. Trucks, H. B. Schlegel *et al.*, GAUSSIAN 03, revision C.02, Gaussian, Inc., Wallingford, CT, 2004.
[45] A. D. Becke, Phys. Rev. A **38**, 3098 (1988).
[46] A. D. Becke, J. Chem. Phys. **98**, 5648 (1993).
[47] C. Lee, W. Yang, and R. G. Parr, Phys. Rev. B **37**, 785 (1988).
[48] S. H. Vosko, L. Wilik, and M. Nusair, Can. J. Phys. **58**, 1200 (1980).
[49] W. H. Press, B. P. Flannery, S. A. Teukolsky, and W. T. Vetterling, *Numerical Recipes in Fortran* (Cambridge University Press, Cambridge, 1992).
[50] N. Troullier and J. L. Martins, Phys. Rev. B **43**, 1993 (1991).
[51] S. J. Weiner, P. A. Kollman, D. A. Case, U. C. Singh, C. Ghio, G. Alagona, S. Profeta, Jr., and P. Weiner, J. Am. Chem. Soc. **106**, 765 (1984).
[52] G. J. Tawa, R. L. Martin, and L. R. Pratt, Int. J. Quantum Chem. **64**, 143 (1997).
[53] G. J. Tawa, R. L. Martin, L. R. Pratt, and T. V. Russo, J. Phys. Chem. **100**, 1515 (1996).